ACS APPLIED MATERIALS & INTERFACES

Letter

www.acsami.org

Polypyrrole-Based Implantable Electroactive Pump for Controlled Drug Microinjection

Bingxi Yan,[†] Boyi Li,[†] Forest Kunecke,[†] Zhen Gu,[‡,§,⊥] and Liang Guo*[,†,∥]

[†]Department of Electrical and Computer Engineering and [∥]Department of Neuroscience, The Ohio State University, Columbus, Ohio 43210, United States

[‡]Joint Department of Biomedical Engineering, University of North Carolina at Chapel Hill and North Carolina State University, Raleigh, North Carolina 27695, United States

[§]Center for Nanotechnology in Drug Delivery and Division of Molecular Pharmaceutics, UNC Eshelman School of Pharmacy, and [⊥]Department of Medicine, University of North Carolina at Chapel Hill, Chapel Hill, North Carolina 27599, United States

Supporting Information

ABSTRACT: Implantable devices for long-lasting controlled insulin microinjection are of great value to diabetic patients. To address this need, we develop a flexible electroactive pump based on a biocompatible polypyrrole composite film that comprises a polypyrrole matrix and a macromolecular dopant of polycaprolactone-*block*-polytetrahydrofuran-*block*-polycaprolactone. Using phosphate-buffered saline as the electrolyte, this film demonstrates much higher electroactivity and reproducibility than conventional Cl^--doped polypyrrole, making it an excellent actuator for driving an implantable pump. At a driving current density of 1 mA/cm^2, the pump demonstrates a consistent output capacity of 10.5 at 0.35 μL/s over 20 cycles. This work paves the way for the development of an implantable electroactive pump to improve the quality of life of diabetics.

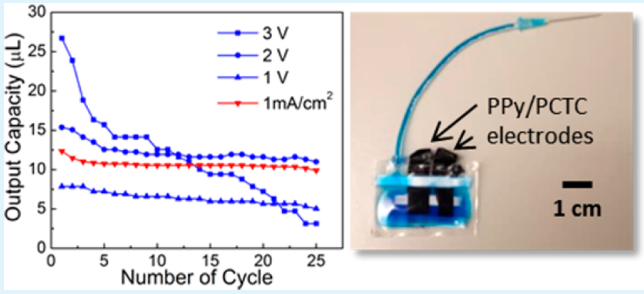

KEYWORDS: *polypyrrole, electroactuator, implantable, controlled drug delivery, diabetes*

Polypyrrole (PPy) has been extensively studied for its capability of producing stress and strain under electrical stimuli. This electroactivity enables its wide use as artificial muscles in robots.[1−4] Transformation of PPy electroactuators stems from ion exchange between the polymer and the surrounding electrolyte during an electrical-induced redox process. PPy with large dopant anions such as $CF_3SO_3^-$, dodecyl benzenesulfonate (DBS), or bis-(trifluoromethanesulfonyl)imide (TFSI) significantly outperforms that with smaller ones such as Cl^- or BF_4^-.[5−8] However, these large dopants are inherently toxic, preventing their use in implantable PPy. Additionally, for optimal performance, these large anion-doped PPy electroactuators require the electrolyte to contain solutes such as LiTFSI, $NaPF_6$, or $LiClO_4$, a condition that cannot be met in in vivo application, where the physiological electrolyte is enriched with Na^+ and Cl^-. Although recent progress on solid-state PPy devices suggests the possibility of encapsulating a biohazard electrolyte into a sandwiched multilayer structure, safety concerns still preclude this approach from being considered for in vivo application.[9−12] Recently, Yang et al. reported their success in driving PPy actuators wirelessly based on a flexible rectenna array, which facilitates the design of a fully implantable device but again requires biocompatible PPy actuators that can be effectively driven in a physiological electrolyte.[13]

The present work was motivated by the pressing need of an implantable pump for long-lasting controlled insulin microinjection by diabetic patients. Here, we developed a flexible electroactive pump based on a previously invented PPy composite film, which comprised a PPy matrix and a macromolecular dopant of polycaprolactone-*block*-polytetrahydrofuran-*block*-polycaprolactone (hereafter named a PPy/PCTC composite).[14,17] This PPy/PCTC composite distinguished itself in biocompatibility as well as significant and reproducible electroactivity in a physiological electrolyte. The resulting pump demonstrated a consistent output capacity of 10.5 at 0.35 μL/s over 20 cycles at an optimal driving current density of 1 mA/cm^2, suitable for microinjection of highly concentrated insulin such as U-500 (500 units/mL, 10−30 μL required per meal by most patients).[15,16] Although both the lifetime and output capacity need further optimization for long-term in vivo application, this work showcased the PPy/PCTC film as a superior electroactuator in a physiological environment and will inspire the future design of more sophisticated implantable devices. Our ultimate goal is to develop a

Received: May 25, 2015
Accepted: July 2, 2015
Published: July 2, 2015

DOI: 10.1021/acsami.5b04551
ACS Appl. Mater. Interfaces 2015, 7, 14563−14568

subcutaneous electroactive pump to improve the quality of life of diabetic patients who need additional hormone.

The electrochemical synthesis, chemical structure, and mechanical properties of the PPy/PCTC composite had been reported previously.[14,17] The synthesized PPy/PCTC film had a thickness of 10 μm with a shiny black surface (Figure 1a).

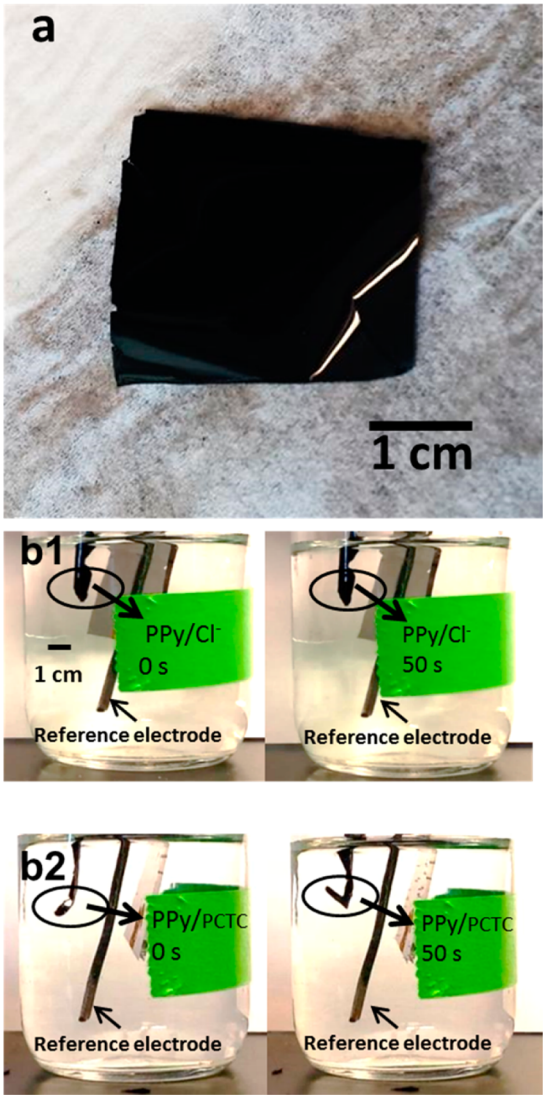

Figure 1. PPy/PCTC composite and its electroactuation in PBS. (a) Photograph of a PPy/PCTC film. (b) Deformation under 2 V after 50 s. b1: no visible deformation for the PPy/Cl^- film. b2: large deformation observed for the PPy/PCTC film.

When driven at 2 V in phosphate-buffered saline (PBS) for 50 s, the PPy/PCTC film displayed a much more remarkable deformation than the conventional PPy/Cl^- film (Figure 1b). As a measure, when the voltage applied on the 5 mm × 15 mm PPy/PCTC strip shifted from +2 to −2 V, after 30 s, a bending angle of 42° was observed, whereas deformation of PPy/Cl^- could barely be seen. (Electroactuation of a PPy/PCTC strip in PBS is presented in the video in the Supporting Information.) This is in agreement with prior reports that PPy/Cl^- can only yield a very small deformation because of its limited ion size.[6,18] The negatively charged flexible PCTC network incorporated into the positively charged rigid PPy matrix acts as the counterion, similar to Cl^- in PPy/Cl^-.[19]

For PPy/Cl^- to function within its breakdown limits, starting with oxidation, additional anions from the electrolyte (PBS) are absorbed into the PPy matrix, causing swelling. During the subsequent reduction phase, the absorbed alien anions together with the native Cl^- dopants gradually diffuse out of the PPy matrix, potentially leading to recovery from the small swelling yet unobservable here. When reduction proceeds beyond the original electrochemical equilibrium, the PPy matrix continues to expel the anions into the electrolyte, resulting in shrinking. Further reduction is likely to cause the PPy matrix to absorb cations from the electrolyte. Returning to another oxidation phase, any absorbed cations are expelled and anions including Cl^- from the electrolyte are doped in the PPy matrix again, leading to recovery from shrinking. Removal of the external driving voltage at any time point could not restore PPy/Cl^- to its original electrochemical state because of exchange of the doping Cl^- with alien anions from the electrolyte, a degrading process causing an irreversible change to the original chemical structure of the polymer. Therefore, doping and dedoping of anions are the dominant mechanism accountable for deformation of PPy/Cl^-.

In contrast, for PPy/PCTC to function within its breakdown limits, during oxidation, anions from the electrolyte (PBS) are absorbed into the PPy/PCTC matrix, but the PPy matrix develops stronger attractions to the bound PCTC network, causing contraction of the film. During the subsequent reduction phase, the absorbed anions are expelled out of the PPy matrix, and PPy/PCTC recovers from contraction. When PPy/PCTC is further reduced beyond the original electrochemical equilibrium, the negatively charged PCTC network is unbound from, but still stuck within, the reduced PPy matrix because of its large size and entanglement with the PPy matrix.[17] Strong spatial remodeling between the unbound PCTC network and the PPy matrix is believed to cause a remarkable expansion of the film. Meanwhile, to maintain charge neutrality, the PPy/PCTC matrix absorbs small cations like Na^+ and K^+ from the electrolyte. Returning to another oxidation phase, the PCTC network reassociates with the PPy matrix and the alien cations are gradually expelled from the PPy/PCTC matrix, leading to recovery from expansion. Removal of the external driving voltage at any time point resets PPy/PCTC to its original electrochemical state, with all alien ions expelled from the polymer matrix, a reversible process causing no change to the original chemical structure of the polymer, which also accounts for slow degradation of the material's electroactivity.

Figure 2a shows a comparison on the charge exchange efficiency between these two types of PPy, which partially explains the disparity in the observed deformations. Apparently, the PPy/Cl^- film had a rather small capacity for reversible faradaic charge transfer, as indicated by the small conductance, which had also been observed by others.[18] The large deformation in PPy/PCTC presumably resulted from strong spatial interactions between the PCTC network and the PPy matrix caused by the large amount of transferred reversible faradaic charges.

Figure 2b shows cyclic voltammograms of PPy/PCTC and PPy/Cl^- in PBS at ±3 V, which confirm that PPy/PCTC had a much higher charge-transfer capacity than PPy/Cl^-. It is worth noting that, when the scanning voltage was applied between two PPy/PCTC electrodes, we observed no gas generation even at a voltage amplitude of up to 5 V. In contrast, when platinum or stainless steel was used as the counter electrode,

DOI: 10.1021/acsami.5b04551
ACS Appl. Mater. Interfaces 2015, 7, 14563−14568

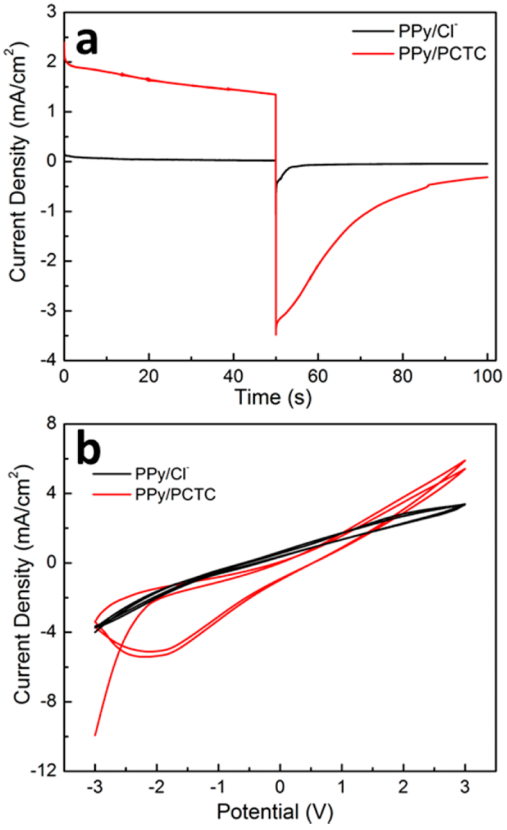

Figure 2. Electrochemical characteristics of PPy/PCTC and PPy/Cl^-. (a) Current density under ±2 V voltage driving with each phase of 50 s. (b) Cyclic voltammograms of PPy/PCTC in PBS at a scan rate of 50 mV/s, in comparison to those of PPy/Cl^-. The reference electrode was Ag/AgCl.

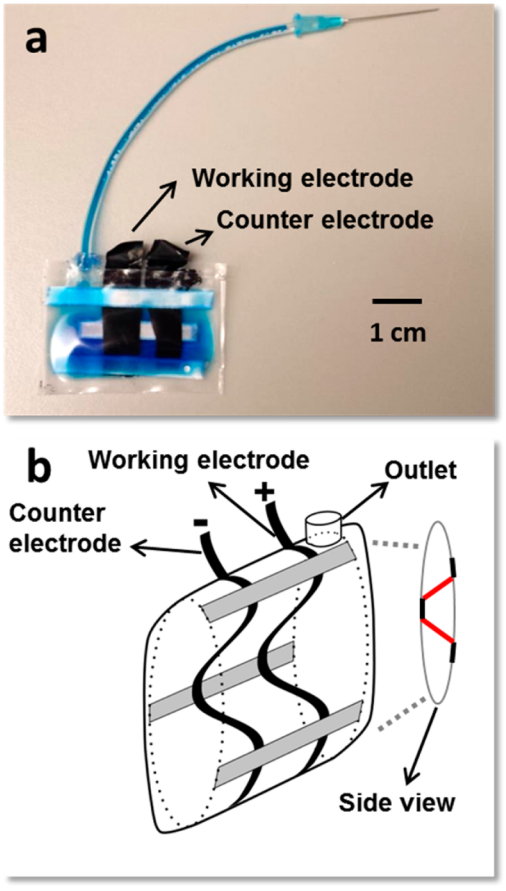

Figure 3. Fully assembled electroactive pump. (a) Photograph of the device. Methylene blue was added for fluid visualization. (b) Schematic illustration of the structure. PBS and PPy/PCTC electrodes were sealed with polyethylene membranes. Gray strips: polypropylene double-sided tape. The side view illustrates the zigzag configuration of the PPy/PCTC working electrode attached alternatively on the pump's inner surfaces; contraction of the red sections generates a squeezing force.

deformation of the PPy/PCTC film (i.e., the working electrode) was always accompanied by gas generation only on the counter electrode for driving voltages exceeding the water electrolysis window (−0.6 to +0.8 V for Pt). Apparently, the effective voltage at the PPy/PCTC−electrolyte interface did not exceed the limits for water electrolysis even with 5 V between the two electrodes. Compared to metal electrodes, a sizable ohmic voltage drop in the semiconductive PPy/PCTC (conductivity of the dry film: 116.3 ± 7.8 S/cm)[14] and a large voltage across the reversible faradaic resistance at the electrode−electrolyte interface likely explain the absence of gas generation (i.e., water electrolysis). However, at an excess driving voltage, it is also possible that some irreversible redox reactions in the PPy backbones take place before water can electrolyze, thus causing deterioration to the polymer structure. Nonetheless, such a strong tolerance of PPy/PCTC to the applied voltage allows us to employ moderate driving voltages beyond the water electrolysis window to drive PPy/PCTC actuators.

Figure 3 shows a prototype of our electroactive pump, where all materials used are biocompatible. Aiming for subcutaneous implantation, the pump was designed as a planar structure of 40 mm × 30 mm × 2 mm (average thickness; the middle is thicker than the edges), yielding a total volume of 2.4 mL. The flat pump consisted of a polyethylene capsule with two 7 × 25 mm PPy/PCTC electrodes assembled in parallel. As illustrated in Figure 3b, each PPy/PCTC electrode was attached alternatively between the pump's two inner surfaces, giving a zigzag configuration. When the pump was filled with PBS and a driving voltage was applied between the two electrodes, this configuration proved highly efficient in compressing the pump to produce a notable and reproducible volumetric output. It was observed that the thicker middle of the pump was much easier to squeeze than the edges. Therefore, the electrode in the middle was used as the working electrode, and as shown in the side view in Figure 3b, its contraction squeezed the pump. The other electrode close to the edge had limited influence on the pump's output and therefore could be replaced by a flat electrode without causing much difference on the output capacity. As a cycle began, the working electrode driven by a positive voltage underwent oxidation and contracted as a result of stronger attractions developed between the PPy backbones and the bound PCTC network (see above for an explanation of the mechanism), generating a force squeezing out the solution, whereas the counter electrode underwent reduction and expanded primarily because of spatial remodeling between the unbound PCTC network and the PPy backbones. When the polarity of the driving voltage was reversed, both electrodes gradually recovered from deformation and thus the pump became relaxed. We call this compression (driven by a positive voltage) and subsequent recovery (driven by a negative voltage of the same amplitude) of the pump a *cycle*. To calibrate the

DOI: 10.1021/acsami.5b04551
ACS Appl. Mater. Interfaces 2015, 7, 14563−14568

output volume at a high accuracy, a glass capillary (internal diameter 1.2 mm; not shown in Figure 3a) was mounted on the pump's outlet, so that it served as a direct volumetric index to changes of the liquid volume inside.

Figure 4 shows evolutions of the output capacity at driving conditions of 3, 2, and 1 V and 1 mA/cm^2. The maximum

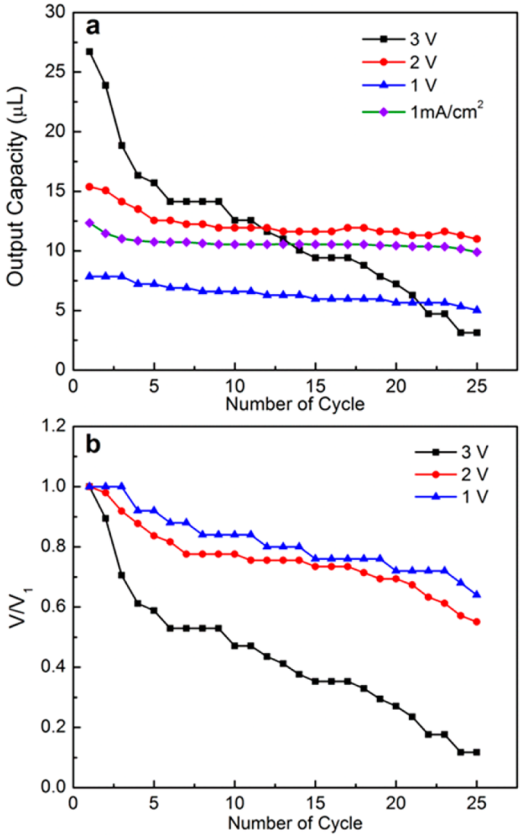

Figure 4. Evolution of the output capacity. Different pumps were used for measurement at each driving voltage. (a) Evolutions of the output capacity at different driving voltages, where each cycle began with a positive voltage between the working and counter electrodes for 30 s and then switched to a negative voltage for another 30 s. The diamond line indicates the output at a constant current density of 1 mA/cm^2. (b) Evolutions of the output capacity normalized to the first cycle, where V_1 is the output volume by 30 s of the first cycle.

output capacities (i.e., the output volume by 30 s of the first cycle) were 26.5, 15.8, 7.5, and 12.4 μL, respectively. This result agreed with our observation that PPy/PCTC films driven at a higher voltage in PBS produced a larger deformation. However, it does not suggest that the pump simply favors a high driving voltage. One main issue with a high driving voltage is fast degradation of PPy/PCTC's electroactive performance due to overoxidation and -reduction to the PPy backbones, which may lead to irreversible damage to the polypyrrole backbones.[20−23] Specifically, we found that, after 25 cycles driven at 3 V, the pump could only retain 18.1% of its first output capacity (V_1). In contrast, at driving voltages of 2 and 1 V, after 25 cycles the pump retained 63.5% and 65.3% of its V_1, respectively. This result suggests that we should make a trade-off between the output capacity and the functional lifetime of the pump. Specifically, to achieve a decent lifetime longer than 20 cycles, the driving voltage should be set below 2 V.

Figure 5a reveals degradation of the charge-transfer capacity of the PPy/PCTC working electrode over consecutive cycles in

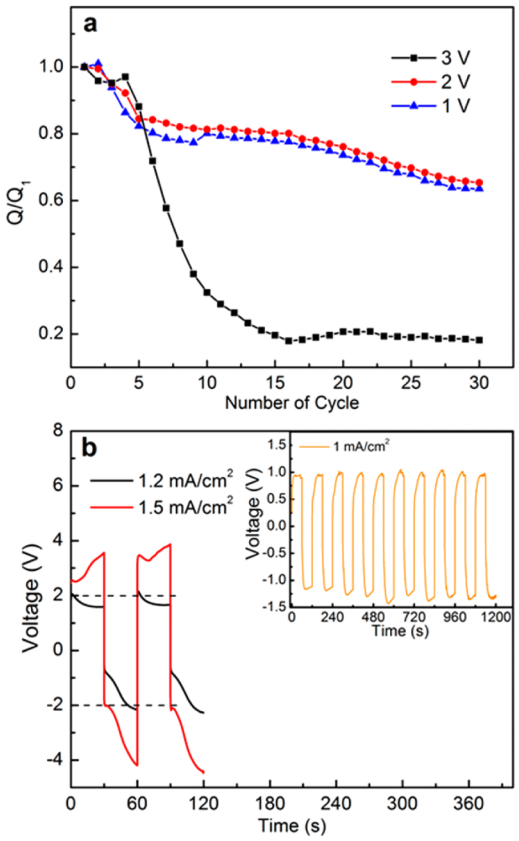

Figure 5. Degradation of the charge-transfer capacity and voltage response in a constant-current driving mode. (a) Degradation of the charge-transfer capacity in the experiment in Figure 4. Q_1 is the total amount of charges transferred by 30 s of the first cycle. (b) Voltage response in a constant-current driving mode. Inset: voltage evolution during the first 10 cycles at a driving current density of 1 mA/cm^2. Note that each cycle was 120 s.

the experiment in Figure 4. When a positive voltage was applied between the working and counter electrodes in the first half of a cycle, PPy backbones in the working electrode underwent oxidation and developed stronger attractions to the PCTC network, leading to contraction of the electrode, while PPy/PCTC absorbed additional anions from the electrolyte. Therefore, the amount of positive charges transferred from the working electrode into PBS in the first half of a cycle indicated the extent of contraction by the working electrode and thus determined the output capacity. As the second half of the cycle began, the working and counter electrodes recovered both electrochemically and mechanically. Unfortunately, because the PPy backbones were gradually overoxidized and/or -reduced through cycles,[20,22,23] the charge-transfer and output capacities degraded correspondingly. Impressively, degradation of the charge-transfer capacities in Figure 5a correlates well with degradation of the output capacities in Figure 4b, which substantiates that the maximum displacement of the PPy/PCTC working electrode was determined by the maximum amount of positive charges transferred from the working electrode to PBS during the first half of a cycle (the compressing phase).

DOI: 10.1021/acsami.5b04551
ACS Appl. Mater. Interfaces 2015, 7, 14563−14568

In the constant-current driving mode for a cycle with a duration of t, the maximally transferred positive charges Q from the working electrode into PBS (the charge-transfer capacity) are equal to $I \times t/2$ and therefore can be identified by the current I. This implies that, ideally for a cycle, a constant current density can deliver a constant amount of charges and thereby achieve a constant pump output. Here, we further tested the pump in the constant-current driving mode. According to Figure 4, to avoid fast degradation to the performance, the amplitude of the driving voltage between the two PPy/PCTC electrodes should be kept below 2 V. Figure 5b shows the voltage response in the constant-current mode. The voltage amplitude required for sustaining a constant current density of 1.5 mA/cm^2 exceeded 2 V even upon onset. At 1.2 mA/cm^2, the voltage amplitude could be maintained within the tolerance range. Therefore, in the inset, a current density of 1 mA/cm^2 was used. The maximum amplitudes of the voltage response for the first 10 cycles were successfully maintained below 1.5 V, even if the cycle period was increased to 60 s. As shown in Figure 4a, the pump outputs under this condition almost leveled over the cycles. This result validated the feasibility of maintaining a consistent output capacity by a constant driving current for a fixed duration. However, as shown in the inset of Figure 5b, gradual increases of the maximum voltage amplitudes over cycles indicated progressive deterioration to the PPy backbones, a mechanism also responsible for degradations of the output capacity in Figure 4 and the charge-transfer capacity in Figure 5a.

Within PPy/PCTC's breakdown limits, redox reactions generated by electrical stimulation are restricted to the reversible faradaic charge transfer in the PPy backbones; alien ions from the electrolyte flow in and out, depending on the state of the PPy backbones; the PCTC network remains stuck within the PPy matrix.[17] So, electroactuation of the PPy/PCTC electrodes causes little disturbance to the physiological environment and the loaded drug. However, it is possible that, even at a driving voltage of 1 V for the duration investigated, the PPy backbones were driven to progressively deteriorate, as indicated by degradation of the charge-transfer capacity over cycles in Figure 5a. Fortunately, products from electrodecomposition of the PPy backbones are biocompatible.[24] Furthermore, our previous rat subcutaneous implantation study had revealed better biocompatibility of PPy/PCTC than that of PPy/Cl$^-$, which is widely considered biocompatible.[25] Therefore, our electroactive pump is particularly promising for in vivo application.

In conclusion, we have developed an implantable electroactive pump using a PPy/PCTC composite film as the electroactuator. The pump demonstrated a consistent output capacity of 10.5 at 0.35 μL/s over 20 cycles at an optimal driving current density of 1 mA/cm^2, suitable for microinjection of therapeutics requiring precise doses, such as U-500. Leveraging the excellent biocompatibility of PPy/PCTC, the pump is promising for in vivo application. Future work will include optimizing the pump's design and driving protocol and performing implantation studies in a small animal model to develop a subcutaneous electroactive pump to improve the quality of life of diabetics.[26]

■ ASSOCIATED CONTENT

Supporting Information

Experimental details and a video of the electroactive response of a PPy/PCTC film in PBS. The Supporting Information is available free of charge on the ACS Publications website at DOI: 10.1021/acsami.5b04551.

■ AUTHOR INFORMATION

Corresponding Author

*E-mail: guo.725@osu.edu.

Notes

The authors declare no competing financial interest.

■ ACKNOWLEDGMENTS

This work was partially supported by The Ohio State University Materials Research Seed Grant Program, funded by the Center for Emergent Materials, an NSF-MRSEC, Grant DMR-1420451, the Center for Exploration of Novel Complex Materials, and the Institute for Materials Research.

■ REFERENCES

(1) Otero, T. F.; Broschart, M. Polypyrrole Artificial Muscles: a New Rhombic Element. Construction and Electrochemomechanical Characterization. *J. Appl. Electrochem.* **2006**, *36*, 205−214.

(2) Otero, T. F. Reactive Conducting Polymers as Actuating Sensors and Tactile Muscles. *Bioinspiration Biomimetics* **2008**, *3*, 035004.

(3) Kiefer, R.; Kilmartin, P. A.; Bowmaker, G. A.; Cooney, R. P.; Travas-Sejdic, J. Actuation of Polypyrrole Films in Propylene Carbonate Electrolytes. *Sens. Actuators, B* **2007**, *125*, 628−634.

(4) Asaka, K.; Mukai, K.; Sugino, T.; Kiyohara, K. Ionic Electroactive Polymer Actuators Based on Nano-carbon Electrodes. *Polym. Int.* **2013**, *62*, 1263−1270.

(5) Bay, L.; West, K.; Sommer-Larsen, P.; Skaarup, S.; Benslimane, M. A. Conducting Polymer Artificial Muscle with 12% Linear Strain. *Adv. Mater.* **2003**, *15*, 310−313.

(6) Hara, S.; Zama, T.; Takashima, W.; Kaneto, K. TFSI-doped Polypyrrole Actuator with 26% strain. *J. Mater. Chem.* **2004**, *14*, 1516−1517.

(7) Kaneto, K.; Fujisue, H.; Kunifusa, M.; Takashima, W. Conducting Polymer Soft Actuators Based on Polypyrrole Films-energy Conversion Efficiency. *Smart Mater. Struct.* **2007**, *16*, S250−S255.

(8) Entezami, A. A.; Massoumi, B. Artificial Muscles, Biosensors and Drug Delivery Systems based on Conducting Polymers: a Review. *Iran. Polym. J.* **2006**, *15*, 13−20.

(9) Asaka, K.; Mukai, K.; Sugino, T.; Kiyohara, K. Ionic Electroactive Polymer Actuators based on Nano-carbon Electrodes. *Polym. Int.* **2013**, *62*, 1263−1270.

(10) Mahadeva, S. K.; Kim, J. Nanocoating of Ionic Liquid and Polypyrrole for Durable Electro-active Paper Actuators Working under Ambient Conditions. *J. Phys. D: Appl. Phys.* **2010**, *43*, 205502.

(11) Naficy, S.; Stoboi, N.; Whitten, P. G.; Spinks, G. M.; Wallace, G. G. Evaluation of Encapsulating Coatings on the Performance of Polypyrrole Actuators. *Smart Mater. Struct.* **2013**, *22*, 075005.

(12) Madden, J. D.; Cush, R. A.; Kanigan, T. S.; Hunter, I. W. Fast Contracting Polypyrrole Actuators. *Synth. Met.* **2000**, *113*, 185−192.

(13) Yang, S. Y.; Mahadeva, S. K.; Kim, J. Wirelessly Driven Electroactive Paper Actuator Made with Cellulose-polypyrrole-ionic Liquid and Dipole Rectenna. *Smart Mater. Struct.* **2010**, *19*, 105026.

(14) Guo, L.; Ma, M. M.; Zhang, N.; Langer, R.; Anderson, D. G. Stretchable Polymeric Multielectrode Array for Conformal Neural Interfacing. *Adv. Mater.* **2014**, *26*, 1427−1433.

(15) Cochran, E.; Gorden, P. Use of U-500 Insulin in the Treatment of Severe Insulin Resistance. *Insulin* **2008**, *3*, 211−218.

(16) Quinn, S. I.; Lansang, C.; Mina, D. Safety and Effectiveness of U-500 Insulin Therapy in Patients with Insuliln-resistant Type 2 Diabetes Mellitus. *Pharmacotherapy* **2011**, *31*, 695−702.

(17) Ma, M. M.; Guo, L.; Anderson, D. G.; Langer, R. Bio-inspired Polymer Composite Actuator and Generator Driven by Water Gradients. *Science* **2013**, *339*, 186−189.

DOI: 10.1021/acsami.5b04551
ACS Appl. Mater. Interfaces 2015, 7, 14563−14568

(18) Johanson, U.; Marandi, M.; Sammelselg, V.; Tamm, J. Electrochemical Properties of Porphyrin-doped Polypyrrole Films. *J. Electroanal. Chem.* **2005**, *575*, 267−273.
(19) Ansari, R. Polypyrrole Conducting Electroactive Polymers: Synthesis and Stability Studies. *E. J. Chem.* **2006**, *3*, 186−201.
(20) Zelikin, A. N.; Lynn, D. M.; Farhadi, J.; Martin, I.; Shastri, V.; Langer, R. Erodible Conducting Polymers for Potential Biomedical Applications. *Angew. Chem.* **2002**, *114*, 149−152.
(21) Otero, T.; Tejada, R.; Elola, A. Formation and Modification of Polypyrrole Films on Platinum Electrodes by Cyclic Voltammetry and Anodic Polarization. *Polymer* **1987**, *28*, 651−658.
(22) Park, D.-S.; Shim, Y.-B.; Park, S.-M Degradation of Electrochemically Prepared Polypyrrole in Aqueous Sulfuric Acid. *J. Electrochem. Soc.* **1993**, *140*, 609−614.
(23) Beck, F.; Braun, P.; Oberst, M. Organic Electrochemistry in the Solid State-Overoxidation of Polypyrrole. *Ber. Bunsenges. Phys. Chem.* **1987**, *91*, 967−974.
(24) Zelikin, A. N.; Lynn, D. M.; Farhadi, J.; Martin, I.; Shastri, V.; Langer, R. Erodible Conducting Polymers for Potential Biomedical Applications. *Angew. Chem.* **2002**, *114*, 149−152.
(25) George, P. M.; Lyckman, A. W.; LaVan, D. A.; Hegde, A.; Leung, Y.; Avasare, R.; Testa, C.; Alexander, P. M.; Langer, R.; Sur, M. Fabrication and Biocompatibility of Polypyrrole Implants Suitable for Neural Prosthetics. *Biomaterials* **2005**, *26*, 3511−3519.
(26) Mo, R.; Jiang, T. Y.; Di, J.; Tai, W. Y.; Gu, Z. Emerging Micro- and Nanotechnology based Synthetic Approaches for Insulin Delivery. *Chem. Soc. Rev.* **2014**, *43*, 3595−3629.

■ NOTE ADDED AFTER ASAP PUBLICATION

This paper was published on the Web on July 6, 2015. Additional text corrections were received, and the paper was reposted on July 7, 2015.

DOI: 10.1021/acsami.5b04551
ACS Appl. Mater. Interfaces 2015, 7, 14563−14568